

# A measurement of the Alcock-Paczynski effect using cosmic voids in the SDSS

P. M. Sutter<sup>1,2,3</sup> <sup>\*</sup>, Alice Pisani<sup>1,2</sup>, Benjamin D. Wandelt<sup>1,2,4,5</sup>, and David H. Weinberg<sup>6,3</sup>

<sup>1</sup> Sorbonne Universités, UPMC Univ Paris 06, UMR7095, Institut d’Astrophysique de Paris, F-75014, Paris, France

<sup>2</sup> CNRS, UMR7095, Institut d’Astrophysique de Paris, F-75014, Paris, France

<sup>3</sup> Center for Cosmology and AstroParticle Physics, Ohio State University, Columbus, OH 43210

<sup>4</sup> Department of Physics, University of Illinois at Urbana-Champaign, Urbana, IL 61801

<sup>5</sup> Department of Astronomy, University of Illinois at Urbana-Champaign, Urbana, IL 61801

<sup>6</sup> Department of Astronomy, Ohio State University, Columbus, OH 43210

23 July 2014

## ABSTRACT

We perform an Alcock-Paczynski test using stacked cosmic voids identified in the SDSS Data Release 7 main sample and Data Release 10 LOWZ and CMASS samples. We find  $\sim 1,500$  voids out to redshift 0.6 using a heavily modified and extended version of the watershed algorithm ZOBOV, which we call VIDE (Void IDentification and Examination). To assess the impact of peculiar velocities we use the mock void catalogs presented in Sutter et al. (2013). We find a constant uniform flattening of 14% along the line of sight when peculiar velocities are included. This flattening appears universal for all void sizes at all redshifts and for all tracer densities. We also use these mocks to identify an optimal stacking strategy. After correcting for systematic effects we find that our Alcock-Paczynski measurement leads to a preference of our best-fit value of  $\Omega_M \sim 0.15$  over  $\Omega_M = 1.0$  by a likelihood ratio of 10. Likewise, we find a factor of 4.5 preference of the likelihood ratio for a  $\Lambda$ CDM  $\Omega_M = 0.3$  model and a null measurement. Taken together, we find substantial evidence for the Alcock-Paczynski signal in our sample of cosmic voids. Our assessment using realistic mocks suggests that measurements with future SDSS releases and other surveys will provide tighter cosmological parameter constraints. The void-finding algorithm and catalogs used in this work will be made publicly available at <http://www.cosmicvoids.net>.

**Key words:** cosmology: observations, cosmology: large-scale structure of universe, cosmology: cosmological parameters, methods: data analysis

## 1 INTRODUCTION

Alternative cosmological probes offer complementary and orthogonal avenues for answering pressing questions such as the nature of dark energy and the growth of large-scale structure (for a recent review of traditional and alternative probes, see Weinberg et al. 2013). One such alternative probe is the Alcock-Paczynski (AP) test (Alcock & Paczynski 1979), which instead of using standard candles such as Type Ia supernovae (e.g., Aldering et al. 2002) or standard rulers such as baryon acoustic oscillations (BAO; Anderson et al. 2012) relies on standard *spheres* for a geometrical test of cosmological parameters. The principal concept underlying the AP test is simple: in a properly chosen cosmology, spheres

will maintain a uniform ratio of line-of-sight to angular extent. Deviations from sphericity as a function of redshift thus reveal the true cosmology.

Since the AP test relies only on statistical isotropy, it has been considered for — and applied to — a variety of systems and features, such as the Lyman- $\alpha$  forest (Hui et al. 1999; McDonald & Miralda-Escudé 1999; Eriksen et al. 2005), the power spectrum of the epoch of reionization (Nusser 2005), galaxy cluster autocorrelation spectra (Kim & Croft 2007), galaxy clustering in the WiggleZ survey (Blake et al. 2011), galaxy pairs (Jennings et al. 2012), and the BAO feature in the Sloan Digital Sky Survey (Reid et al. 2012).

Current successful applications of the AP test (e.g., Blake et al. 2011; Reid et al. 2012) are limited to large scales, fundamentally limiting their constraining power. A promis-

<sup>\*</sup> Email: [sutter@iap.fr](mailto:sutter@iap.fr)

ing way to apply the AP test to smaller scales (thereby reducing statistical uncertainties) while still avoiding large systematics is to use cosmic voids (Lavaux & Wandelt 2012), the large underdense regions in the cosmic web (Thompson & Gregory 2011). Voids offer potentially revolutionary potential: in terms of statistical power Lavaux & Wandelt (2012) predicted that the AP test applied with voids in the upcoming Euclid survey (Laureijs et al. 2011) will outperform BAO in constraining dark energy equation of state parameters by up to a factor of ten.

The power of voids comes from two aspects. First, their small size compared to the BAO feature, down to  $\sim 5 h^{-1}\text{Mpc}$  (Sutter et al. 2012b), gives them significant statistical weight. Second, since their evolution is in the linear or quasi-linear regime, systematic effects due to peculiar velocities will be highly suppressed and easy to model out. Even though the BAO feature is more linear than void features, voids are a collective phenomenon defined by many galaxies and so void profiles (and shapes) are a cross-correlation (Hamaus et al. 2013), whereas the BAO relies on galaxy-galaxy auto-correlation. As we will see in this paper, the cross-correlation has potential to be less affected by peculiar velocities and other systematics than the auto-correlation.

Put simply, voids are simple objects. For example, Hamaus et al. (2014) discovered a single two-parameter density profile that describes voids of all sizes, and Sutter et al. (2013) applied this profile to reveal that voids in theory (e.g., in dark matter simulations) obey self-similar scaling relations to voids in observations (e.g., in galaxy surveys). Also, the merger tree analysis of Sutter et al. (2014) found that voids essentially do not move and do not merge over their lifetimes; evolutionary dynamics do not overwhelm primordial cosmological information.

Even though current galaxy redshift surveys are not optimized for finding large numbers of voids (due to their relative sparsity, low redshift, and complicated survey geometries), cosmological measurements with voids are still possible: for example, the largest publicly-available void catalog<sup>1</sup> (Sutter et al. 2012b, 2013) has enabled observations such as the ISW effect (Planck Collaboration 2013) and gravitational anti-lensing (Melchior et al. 2014). Previously, we applied the AP test methodology described in Lavaux & Wandelt (2012) to voids found in the SDSS DR7 main sample and LRG catalogs (Sutter et al. 2012b), but due to the small number of voids found no statistically significant result (Sutter et al. 2012a).

In this work we extend the void AP analysis to higher redshifts and to more voids using the BOSS Data Release 10 LOWZ and CMASS galaxy catalogs (Ahn et al. 2014). We also use mock catalogs tuned to our observational surveys to examine the systematic impact of peculiar velocities noted in the pure  $N$ -body simulations of Lavaux & Wandelt (2012). We use these mocks to find an optimal binning strategy to increase sensitivity to our potential signal and then use the resulting size bins on the data.

In Section 2 we describe the galaxy samples and void catalogs to be used in the AP analysis. We discuss our method for measuring distortions in void shapes and the

application to an AP test in Section 3. Section 4 focuses on systematics due to peculiar velocities, while Section 5 features an analysis of our strategy for optimizing the signal given the limited number of voids in our current void catalog. We present our AP results in Section 6 and offer perspectives on future work in Section 7.

## 2 GALAXY & VOID SAMPLES

For each galaxy we transform its sky latitude  $\theta$ , sky longitude  $\phi$ , and redshift  $z$  into a comoving coordinate system:

$$\begin{aligned} x' &= D_c(z) \cos \phi \cos \theta, \\ y' &= D_c(z) \sin \phi \cos \theta, \\ z' &= D_c(z) \sin \theta, \end{aligned}$$

where  $D_c(z)$  is the comoving distance to the galaxy at redshift  $z$ . We assume cosmological parameters consistent with a  $\Lambda$ CDM cosmology as given by the WMAP 7-year results (Komatsu et al. 2011):  $\Omega_M = 0.3$ ,  $\Omega_\Lambda = 0.7$ , and  $h = 0.71$ . We make no corrections for peculiar velocities.

We construct volume-limited galaxy populations by making cuts in magnitude and redshift from the SDSS Data Release 7 main sample (Abazajian et al. 2009) and SDSS-III BOSS Data Release 10 (Ahn et al. 2014) LOWZ and CMASS galaxy catalogs. We make these cuts after applying evolution and  $K$ -corrections and computing absolute magnitudes using the above WMAP 7-year cosmological parameters. The main sample cuts are described more fully in Sutter et al. (2012b), and we split the LOWZ catalog into four samples starting at  $z = 0.1$  and the CMASS catalog into two samples starting at  $z = 0.5$ . To avoid overlap with the DR7 samples we ignore the first lowest-redshift LOWZ sample.

Our void-finding procedure as applied to observational data is described in detail in Sutter et al. (2012b) and Sutter et al. (2013). Briefly, we use a heavily modified version of ZOBOV (Neyrinck 2008; Lavaux & Wandelt 2012; Sutter et al. 2012b, 2013, 2014), which we call **VIDE**, for Void IDentification and Examination. This approach uses a Voronoi tessellation to construct a density field from the galaxy population. Our construction of volume-limited samples ensures that we have uniform density across the void surface so that we do not need to include any weighting in the tessellation step. This density field has topological features such as basins and ridgelines, and **VIDE** assembles adjacent basins into voids using a watershed algorithm. Thus a void is simply an arbitrarily-shaped depression in the density field bounded by high-density ridgelines. **VIDE** does not apply any additional smoothing before the watershed step. In addition to the above references, we will discuss **VIDE** in detail in a forthcoming paper.

A void can have any mean and minimum density, since the watershed algorithm includes as member particles galaxies in the surrounding high-density walls. However, we place a restriction such that the *walls* between adjacent basins cannot be merged into a larger void unless the density of that wall is less than  $0.2\bar{\rho}$ . This prevents the growth of voids deeply into clusters (Neyrinck 2008). Also, we remove voids with central densities greater than  $0.2\bar{\rho}$ , measured within  $1/4$  of the effective void radius. This cleaning aids in the shape measurement below. We only include voids with effective radii greater than the mean galaxy separation.

<sup>1</sup> <http://www.cosmicvoids.net>

**Table 1.** Volume-limited galaxy samples used in this work.

Sample Name	$M_{r,\max}$	$z_{\min}$	$z_{\max}$	$\bar{n}^{-1/3}$ ( $h^{-1}\text{Mpc}$ )	$N_{\text{void}}$
dr72dim1	-18.9	0.0	0.05	3.5	52
dr72dim2	-20.4	0.05	0.1	4.9	174
dr72bright1	-21.4	0.1	0.15	7.4	183
dr72bright2	-22.0	0.15	0.2	12.5	96
dr10lowz2	-19.5	0.2	0.3	13.8	137
dr10lowz3	-20.0	0.3	0.4	15.1	199
dr10lowz4	-20.5	0.4	0.45	16.4	91
dr10cmass1	-19.5	0.45	0.5	14.0	230
dr10cmass2	-19.5	0.5	0.6	15.2	697

Throughout this work we will refer to the void radius. We define the effective radius to be the radius of a sphere with the same volume as the void, where the void volume is the sum of all the Voronoi cell volumes that comprise the void.

To accommodate the survey boundaries and masks we place a large number of mock particles along any identified edge. These mock particles have essentially infinite density and thus prevent the watershed from growing voids outside the survey area. After finding voids we take the *central* selection, where voids are guaranteed to sit well away from any survey boundaries or internal holes: the maximum distance from the void center to any member particle is less than the distance to the nearest boundary. As discussed in Sutter et al. (2012b) and Sutter et al. (2012a), this ensures a fair distribution of void shapes and alignments.

The voids identified with this approach in the DR7 main sample are already publicly available.

Table 1 summarizes the names of our volume-limited samples, the maximum absolute magnitude, redshift bounds, mean galaxy number density, and the total number of voids identified in those samples.

### 3 METHOD

The Alcock-Paczyński (AP) test uses a set of standard spheres to measure cosmological parameters by taking the ratio of line-of-sight distances to angular diameters:

$$\frac{\delta z}{\delta d} = \left( \frac{H_0}{c} \right)^2 \frac{D_A(z)E(z)}{z}, \quad (1)$$

where  $\delta z$  is an extent along the line of sight,  $\delta d$  is an angular extent,  $H_0$  is the Hubble constant,  $D_A(z)$  is the angular diameter distance at redshift  $z$ , and  $E(z)$  is the expansion rate at that redshift. For this work we will assume a flat  $\Lambda$ CDM universe, and thus  $D_A(z)$  becomes

$$D_A(z) = \frac{c}{H_0} \int_0^z \frac{dz'}{E(z')}, \quad (2)$$

with

$$E(z) = (\Omega_m(1+z)^3 + \Omega_\Lambda)^{1/2}. \quad (3)$$

In the above,  $\Omega_m$  and  $\Omega_\Lambda$  are, respectively, the present-day matter and dark energy densities relative to the critical density.

We define the *stretch* parameter  $e_v(z)$  as

$$e_v(z) \equiv \frac{c}{H_0} \frac{\delta z}{\delta d}. \quad (4)$$

While a single void is hardly a standard sphere and inappropriate for the AP test (Ryden 1995), in an isotropic universe voids have no preferred orientation: a *stack* of voids will be a sphere (Lavaux & Wandelt 2012). To stack voids we align their barycenters, which are the volume-weighted centers of all the Voronoi cells in each void:

$$\mathbf{X}_v = \frac{1}{\sum_i V_i} \sum_i \mathbf{x}_i V_i, \quad (5)$$

where  $\mathbf{x}_i$  and  $V_i$  are the positions and Voronoi volumes of each tracer  $i$ , respectively. As we stack, we align the voids so that they share a common line of sight. This same approach has been used to construct real-space density profiles using projections (Pisani et al. 2013). We do not apply any rescalings to the void sizes as we stack.

Thus we can measure the stretch  $e_v(z)$  of stacked voids within independent redshift slices. We placed our galaxy samples into a comoving coordinate system assuming a  $\Lambda$ CDM cosmology. If this is the correct cosmology then the AP test will return unity for all redshifts:  $e_v(z) = 1$ . Deviations from unity as a function of redshift will depend on cosmological parameters (Eq. 1).

To measure the stretch of a stacked void we take all galaxies within a radius cutoff of  $2R_{\max}$ , where  $R_{\max}$  is the maximum void size in the stack. We project these galaxies onto a two-dimensional plane,

$$\begin{aligned} d_v &= \sqrt{x_{\text{rel}}^2 + y_{\text{rel}}^2} \\ z_v &= |z_{\text{rel}}|, \end{aligned} \quad (6)$$

where  $(x_{\text{rel}}, y_{\text{rel}}, z_{\text{rel}})$  are the galaxy coordinates relative to the void barycenter  $\mathbf{X}_v$ :

$$\mathbf{x}_{\text{rel}} \equiv \mathbf{x}' - \mathbf{X}_v. \quad (7)$$

We then transform the line-of-sight coordinate  $z_v$  by a factor  $e_v$  ( $z'_v \equiv e_v z_v$ ) until the ellipticity measured within a sphere of radius  $0.7R_{\max}$  is unity. In testing we found this radius to provide the best balance between gathering as many galaxies as possible for high signal-to-noise while avoiding fluctuations outside the void proper. We will validate this approach in the section below. We calculate the ellipticity  $\epsilon$  via the inertia tensor:

$$\epsilon = \sqrt{\frac{2 \sum z_{v,i}^2}{\sum d_{v,i}^2}}, \quad (8)$$

where the sums are taken over all galaxies within  $0.7R_{\max}$ .

We identify the necessary rescaling factor  $e_v$  as the void stretch which enters into the AP measurement above. To estimate our uncertainty for each stack we repeat the above process for 1,000 bootstrap samples. Figure 1 shows an example void stack taken from the CMASS sample and the measured stretch using this approach.

### 4 ANALYSIS OF SYSTEMATICS

The theoretical analysis of the AP effect with voids discussed in Lavaux & Wandelt (2012) revealed the presence of systematic effects due to peculiar velocities: a uniform compression along the line of sight for voids at all redshifts. In

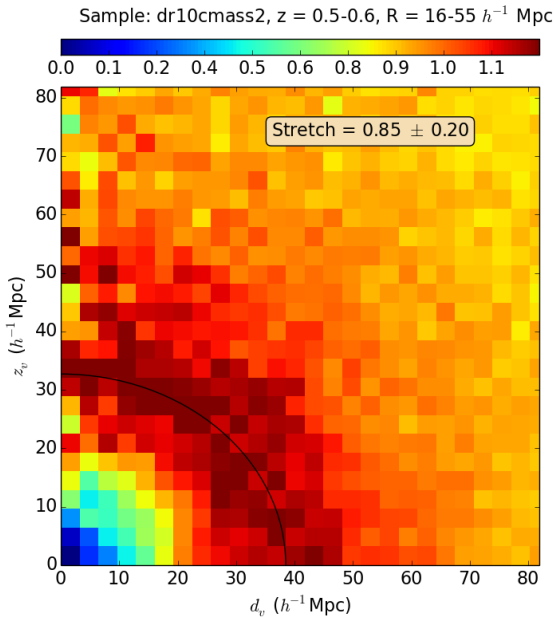


**Figure 1.** Example of a void stack in two dimensions and its stretch measurement. This stack includes voids from size 16 to 55  $h^{-1}$  Mpc. For clarity void galaxies are binned onto a uniform grid with cell size  $\sim 3 h^{-1}$  Mpc, though the bins are not used in the stretch calculation. The black line shows an ellipse with the same stretch as the stacked void, and the caption shows the measured stretch and uncertainty. The uncertainty is the  $1\sigma$  deviation taken from 1,000 bootstrapped samples. The color bar shows the density in each grid cell in units of the mean density of this sample.

order to recover the expected AP signal, a single correction factor of 1.16 (with an observed flattening of 14%, the correction factor is  $1/(1 - 0.14) = 1.16$ ) had to be applied. However, that analysis focused on a relatively thin stack of voids ( $8 - 9 h^{-1}$  Mpc) in a dark matter simulation. We extend this work to examine the impacts of peculiar velocities on more realistic galaxy populations.

For our study we take the publicly-available void population presented in Sutter et al. (2013); namely, the *Halos Dense* and *Halos Sparse* samples. These two void samples are drawn from  $N$ -body simulation halo catalogs with similar number densities (and, by construction, clustering properties) of a high-density galaxy survey such as the DR7 main sample and a low-density survey such as DR10 CMASS, respectively. Note that we do not take the void catalogs drawn from an Halo Occupation Distribution (HOD; Berlind & Weinberg 2002) galaxy population due to the ambiguity in applying HOD modeling at higher redshifts. However, as Sutter et al. (2013) noted, the void populations between halos and galaxies are almost indistinguishable for these kinds of analysis, and thus the halos provide a good proxy for the galaxy populations. The particle positions were perturbed according to their peculiar velocities before finding voids.

We analyze three simulation snapshots at redshifts  $z = 0.05, 0.25$ , and  $0.67$ , and subdivide each snapshot into four slices in the  $z$ -direction. These slices each have a comoving width of  $300 h^{-1}$  Mpc, or  $\Delta z \sim 0.1$ . In total there are

$\sim 25,000$  voids in the *Halos Dense* catalogs and  $\sim 5,000$  in the *Halos Sparse* catalogs. For the *Halos Dense* catalogs, we construct stacks of width  $\Delta R = 10 h^{-1}$  Mpc. The fewer number of voids in the *Halos Sparse* catalogs necessitates the use of wider stacks with  $\Delta R = 40 h^{-1}$  Mpc. We start adding voids to stacks beginning with voids with effective radii equal to the mean particle separation. With these stacks we applied the above AP analysis assuming the  $z$ -direction to be the line of sight.

Figure 2 shows the measured stretch as a function of redshift,  $e_v(z)$ , for these mock setups. Since the voids are drawn from an  $N$ -body simulation with  $\Lambda$ CDM parameters, and we are assuming the same parameters for the AP test, we expect no stretch. Instead, we see the same uniform 14% line-of-sight flattening, and hence a necessary  $e_v(z)$  correction factor of 1.16, as in Lavaux & Wandelt (2012). We indicate this in the figure with a horizontal grey dashed line. We find, but do not show, the expected value of  $e_v(z) = 1.0$  when repeating this analysis on voids without including peculiar velocities.

We see that the systematic flattening due to peculiar velocities first observed by Lavaux & Wandelt (2012) persists for voids in mock galaxy populations, and also persists for all void sizes at all redshifts. There is some indication of a slight deviation for the highest redshifts in the *Halos Sparse* voids, but this is outside the redshift range that we consider in data. These results are not necessarily surprising: the recent works of Hamaus et al. (2014) and Sutter et al. (2013) have shown that a single universal density profile applies to voids in all tracer populations and enables the definition of a scaling relationship among them. Thus it is plausible that systematic effects that impact voids in simulation will be similar in real galaxy populations.

We leave a detailed study of the cause of this systematic offset to future work: a better understanding of this effect can be reached by directly comparing on a one-to-one basis voids in mocks with and without peculiar velocities included (similar to the approach taken in Sutter et al. 2014 to examine the impacts of galaxy sparsity and bias). A preliminary study shows that peculiar velocities impart a uniform flattening to void shapes along the line of sight. While one might expect peculiar velocities to elongate individual voids (Ryden & Melott 1996), the situation is less clear in a statistical sample of the full cosmic web: the elongation in the dynamically outflowing portion of voids competes with a thickening of the walls separating them. In addition, peculiar velocities will have an effect on the assignment of a given portion of survey volume to individual voids.

## 5 OPTIMIZATION

We may use the measured flattening as a metric for optimization: we wish to have as many independent stacks as possible, but too few voids — and hence tracers — in a stack will degrade the shape measurement, leading to  $e_v = 1.0$  even in the presence of peculiar velocities. This occurs because Poisson fluctuations overwhelm the shape distortions caused by Alcock-Paczynski stretching and peculiar velocities. We investigated the minimum number of voids required, the minimum and maximum stack width, the minimum void size to start stacking, the radius at which the ellipticity is

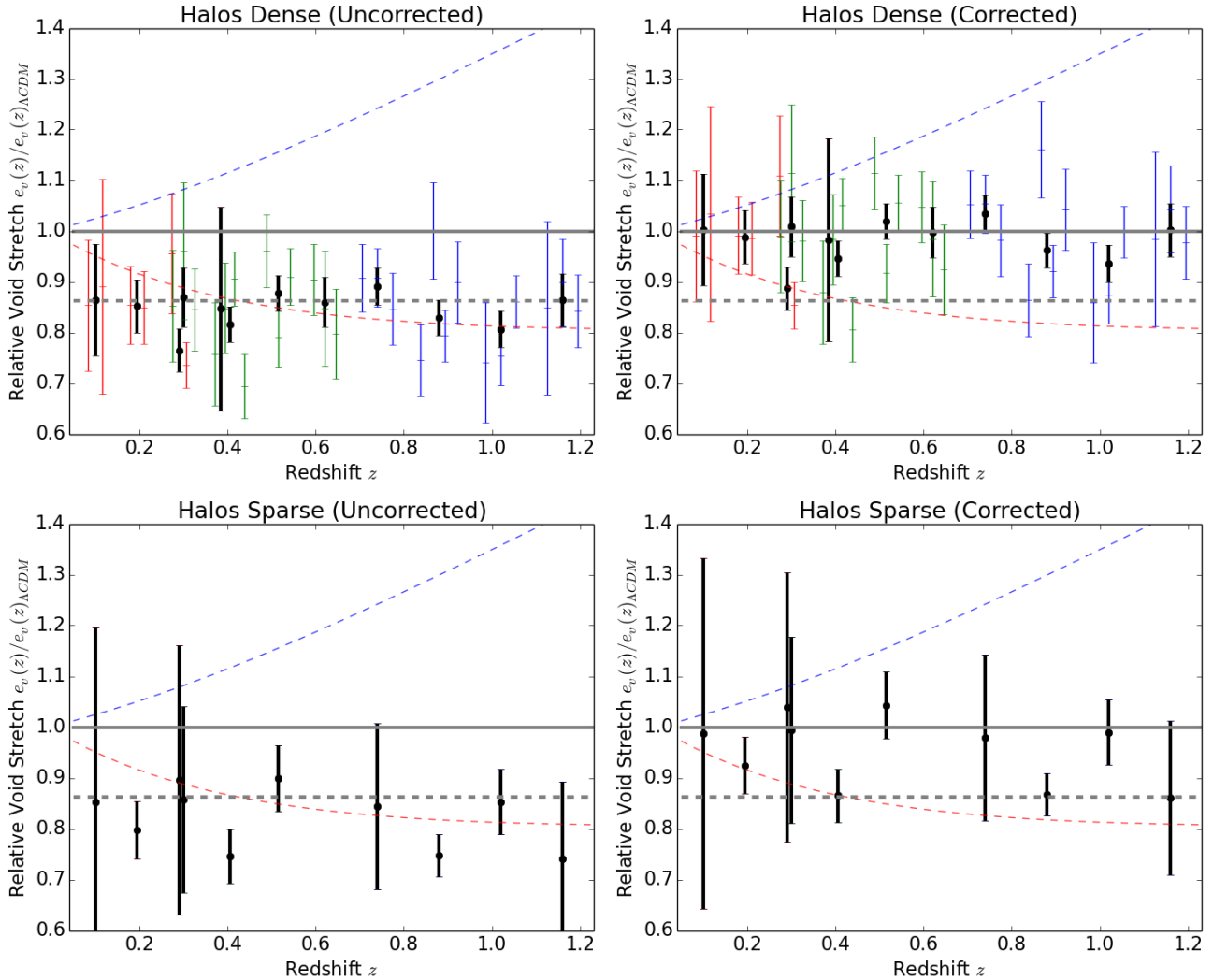


**Figure 2.** Stretch as a function of redshift ( $e_v(z)$ ) relative to the stretch expected in a  $\Lambda$ CDM cosmology for the mock void samples. Since the mocks are drawn from a  $\Lambda$ CDM universe, we expect a stretch measurement of unity, as indicated by the solid grey horizontal line. Peculiar velocities induce a uniform flattening, and the dashed grey line shows the offset found in the dark matter analysis of Lavaux & Wandelt (2012). Each colored point with error bar is the stretch measurement for a single stack (e.g.,  $10 - 15 h^{-1}\text{Mpc}$ ), while the thick black points with error bars are the weighted mean measurements in a redshift slice (if there is only a single stack in the slice we only show the black point with error bar). The individual stack measurements are colored by redshift slice. Different color points correspond to particular simulation snapshots. For reference the dashed blue (red) line corresponds to the relative stretch for an  $\Omega_M = 0.0$  (1.0) universe. The top panels are from the *Halos Dense* mocks and the bottom panels are from the *Halos Sparse* mocks. The left-hand panels are the raw measurement; the right-hand panels show the measurement after applying a uniform correction factor of 1.16.

calculated, whether to use all particles in the stack or only particles that are members of a **VIDE** void, and whether to rescale voids to the same radius or not.

First, we found that rescaling voids severely degrades the measurement due to the broadening of the high-density wall (for example, see the density profiles in Sutter et al. 2012a). This broadening occurs because galaxies are moved to larger radii, leaving fewer galaxies within the void to use for the shape measurement and thereby increasing the Poisson noise. Also, we are able to reliably measure shapes when restricting ourselves to void-galaxies only, but the minimum number of voids in a stack is necessarily larger, since in this case we are making measurements with fewer numbers of particles per void. We found the radius choice of  $0.7R_{\text{max}}$  to be the most robust: at smaller radii we lose too many galax-

ies, and larger radii include fluctuations outside the void wall in the shape estimation, leading to highly variable measurements from stack to stack. When making broad stacks, as we will see below, we found that this criterion still succeeds even when some voids are smaller than  $0.7R_{\text{max}}$  of the stack. Figure 1 shows why this works: in a stacked void without rescaling, small voids contribute to the inner portions of the wall, while larger voids add galaxies to the outer edges. Combined they give a very broad, smooth feature that robustly measures the overall shape.

We found for both catalogs that we may begin stacking at the minimum void size provided by **VIDE**, which is the mean particle separation. We are able to recover reliable stretch measurements when setting larger thresholds for the minimum void size, but with larger statistical uncertainties.

Including all voids down to the mean particle separation did not introduce any systematic error.

For the *Halos Dense* voids we require at least  $\sim 50$  voids per stack to preserve the shape information, while for the *Halos Sparse* voids we must use at least  $\sim 150$  voids per stack. Relatedly, the minimum stack width for reliable measurements in *Halos Dense* was  $\sim 5 h^{-1}\text{Mpc}$ , while in *Halos Sparse* was  $\sim 20 h^{-1}\text{Mpc}$ . We found maximum reliable stack widths of  $\sim 20 h^{-1}\text{Mpc}$  and  $\sim 40 h^{-1}\text{Mpc}$  for the *Halos Dense* and *Halos Sparse* mocks, respectively. The measurement degrades for very wide stacks because we increase the radius at which we compute ellipticities while adding relatively few new voids to the stack.

In addition to the method of general measurement of ellipticity in the stack, we repeated the above analysis for the MCMC shape-fitting algorithm presented in Lavaux & Wandelt (2012) and applied to data in Sutter et al. (2012a), using both a cubic density profile and the universal density profile of Hamaus et al. (2014). With both profiles we are able to reproduce these AP measurements, but we require a factor of  $\sim 2$  greater number of voids per stack to avoid catastrophic failures of the estimator. Also, voids rescaling is required for the profile-fitting method to avoid being dominated by large fluctuations inside the void wall, and rescaling can only be reliably applied for relatively narrow radius bins, as seen above.

While the methods based on profile fitting achieve much tighter constraints once the number of voids is above this threshold, we find ellipticity-based methods such as the one described in Section 3 more robust (i.e., less subject to Poisson noise) for the number of voids available in the extant sample. Also, with relatively few voids available in data we are forced to use wide radial bins, where the profile-fitting method is less robust. We will comment in the Conclusions on the comparison of our results and the forecasts of the AP measurement based on profile-fitting shape measurements.

Finally, we also repeated this analysis in redshift space using the coordinate system of Lavaux & Wandelt (2012) and Sutter et al. (2012a) and found identical results.

## 6 RESULTS

From the above optimization analysis, we selected the stacks listed in Table 2. This table lists the sample name, the void size range in the stack, and the number of voids in the stack. Within each sample we attempted to create as many stacks as possible given the minimum required number of voids in order to correctly estimate the expected stretch in the mocks. We used the *Halos Dense* mock as a guide for the DR7 main sample, and the *Halos Sparse* mock for guidance with the DR10 LOWZ and CMASS samples. We discard the *dr72dim1* and *dr10lowz4* samples due to a lack of a sufficient number of voids. We have verified in mocks that our chosen bin sizes and typical number of voids per stack are able to capture the correct AP measurement (indeed, the stacks used in Figure 2 are capped to 50 and 200 voids for the *Halos Dense* and *Halos Sparse* samples, respectively).

Figure 3 shows our void stretch measurement using the above stacks. In this figure we have already applied the uniform 1.16 correction factor discussed above. We see that after this correction is applied our measurements scatter

**Table 2.** Void stacks used in the analysis.

Sample Name	$R_{\min} - R_{\max} (h^{-1}\text{Mpc})$	$N_{\text{voids}}$
dr72dim2	5 - 8	78
	8 - 12	59
dr72bright1	7 - 12	88
	12 - 20	71
dr72bright2	12 - 28	75
dr10lowz2	14 - 55	135
dr10lowz3	15 - 55	195
dr10cmass1	14 - 55	219
dr10cmass2	16 - 55	659

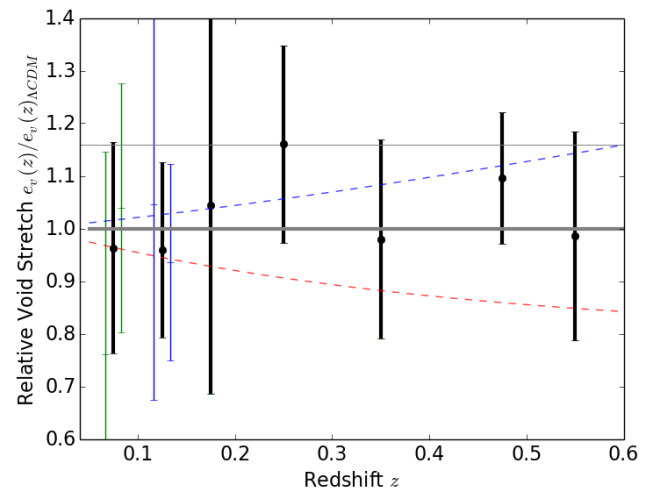


**Figure 3.** Stretch as a function of redshift relative to the expected stretch in a  $\Lambda\text{CDM}$  cosmology (thick solid grey horizontal line) and a null measurement (thin solid grey horizontal line). Each black point with error bars corresponds to the weighted mean measurement in each galaxy sample, while colored points with error bars show individual stack measurements in a single sample, if available. The measurements are already corrected for peculiar velocities using a single 1.16 correction factor, as discussed in Section 4. Error bars are  $1\sigma$  uncertainties obtained using 1,000 bootstrapped samples. For reference the dashed blue (red) line corresponds to the relative stretch for an  $\Omega_M = 0.0$  (1.0) universe.

around the expected value of  $e_v(z) = 1.0$ . These error bars are larger than the mean measurements shown in Figure 2, since in mocks we have many more individual stacks so that the mean measurement has relatively smaller uncertainty. With our limited number of voids in data we have, at best, two stacks per sample.

Note that if our shape measurements were degraded due to an insufficient number of voids in each stack, we would have measured a signal consistent with  $e_v(z) = 1.0$  before correcting for peculiar velocities, and  $e_v(z) = 1.16$  after corrections, since our measurement will be dominated by Poisson noise, as discussed above. For example, the *dr10lowz2* sample has the fewest number of voids for the given sparsity and is the most discrepant from the expected measurement. This serves as a useful null test. To evaluate the significance of our results compared to such a null measurement, we eval-

uate the likelihood ratio

$$K \equiv \frac{\mathcal{L}_{\Lambda\text{CDM}}}{\mathcal{L}_0} = \exp \left[ -\frac{1}{2} (\chi_{\Lambda\text{CDM}}^2 - \chi_0^2) \right], \quad (9)$$

where a subscript of  $\Lambda\text{CDM}$  refers to the expected measurement and a subscript of 0 for a null measurement, and  $\chi^2$  is the residual sum-of-squares. To calculate the likelihood ratio we compute the  $\chi^2$  of our measurements against the expected  $\Lambda\text{CDM}$  model (a constant value of unity for all redshifts) and again against the expected null result (a constant value of 1.16 for all redshifts). The likelihood ratio measures the amount by which our data prefer  $\Lambda\text{CDM}$  to a null measurement.

This significance test assumes Gaussian uncertainties, which is a good approximation to the distribution of our bootstrap samples. Since the expected measurement implicitly assumes some model parameters (namely, the  $\Lambda\text{CDM}$  cosmological parameters) this likelihood ratio is equivalent to a Bayes factor describing the preference of our data being described by a  $\Lambda\text{CDM}$   $\Omega_M = 0.3$  cosmology over a null measurement of constant 1.16 after rescaling. We find  $K = 4.5$ , which while not a very strong rejection of null due to the large error bars, does provide “substantial” evidence, as usually interpreted in the Bayesian literature (Jef 1961). We do not convert this likelihood ratio into a significance since that would require additional modeling of the posterior shape. Our individual  $\chi^2$  measures are less than one, since our error bar estimates should be seen as conservative.

We may also evaluate our measurement by performing a likelihood analysis of various cosmologies assuming the above Gaussian likelihood function. Figure 4 shows the relative likelihood of  $\Omega_M$  values in a flat universe with a cosmological constant, given our stretch measurements. We calculate this likelihood using the weighted average measurements in each redshift bin after correcting for the effects of peculiar velocities. While our error bars do not allow a precise measurement of  $\Omega_M$ , we can read off likelihood ratios for various cosmologies. Most significantly, we disfavor an  $\Omega_M = 1.0$  universe by a factor of  $\sim 10$ , which corresponds to substantial evidence for the AP effect expected in the  $\Lambda\text{CDM}$  model.

## 7 CONCLUSIONS

We have used  $\sim 1,500$  voids identified with the watershed transform code *VIDE* in the SDSS DR7 main sample and BOSS DR10 LOWZ and CMASS samples to perform an Alcock-Paczynski test. We stacked voids to construct standard spheres and measured the ratio of their line-of-sight to angular extents, or *stretch*. We used voids found in mock populations with realistic number densities and clustering properties to assess the impact of peculiar velocities and optimize the stacking to produce the most significant result. After correcting for systematic effects and measuring the void stretch from redshift  $z = 0.05$  to  $0.6$  we translated our Alcock-Paczynski estimation into a constraint on  $\Omega_M$ . We find a best fit value of  $\Omega_M \sim 0.15$ , and our measurements prefer this value over  $\Omega_M = 1.0$  by a factor of 10. We find a likelihood ratio of 4.5 for our results to reject a null measurement. Taken together, we interpret these as a substantial detection of the Alcock-Paczynski test with our sample of cosmic voids.

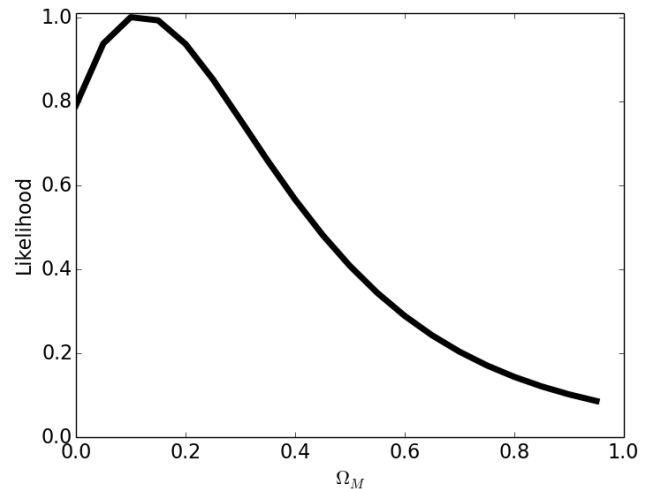


**Figure 4.** One-dimensional relative likelihood as a function of  $\Omega_M$  for our stacked void measurements, after correcting for peculiar velocities.

We have verified the uniform and constant systematic offset caused by peculiar velocities originally seen in the pure  $N$ -body simulations of Lavaux & Wandelt (2012) to also apply to realistic galaxy populations. This 14% line-of-sight flattening appears universal for all void sizes studied ( $7\text{--}80 h^{-1}\text{Mpc}$ ), all redshifts studied ( $z = 0.0\text{--}1.2$ ), and all tracer densities studied ( $3 \times 10^{-4}$  -  $1.0$  particles per cubic  $h^{-1}\text{Mpc}$ ). We observe this flattening regardless of the composition of the void stack, once a minimum threshold number of voids is met. Indeed, the AP measurement is quite binary: either no signal is obtained at all (if there are too few voids) or the measured signal has the expected uniform distortion. While we have some preliminary indication as to the source of this offset, we relegate a full analysis of the effects of peculiar velocities on voids found using *VIDE* to a forthcoming paper.

We used our mocks to find the minimum number of voids necessary in a stack to obtain a measurement and used these results to optimize our result in data. We did not perform an exhaustive search through the space of *all* possible configurations (e.g., optimal number of redshift bins, volume-weighted samples, stacking configurations, etc.) which leaves open the possibility of a substantial improved measurement with current data.

Our previous application of the AP test to cosmic voids (Sutter et al. 2012a) did not correct for systematic effects but did marginalize over potential bias values in the final likelihood analysis, which explains the very large uncertainty and preference for higher  $\Omega_M$  in that analysis.

Based on dark matter simulations Lavaux & Wandelt (2012) predicted that in the full BOSS survey an AP analysis with voids would be competitive with BAO measurements from the same survey set. At this stage our Bayes factor of 4.5 presents substantial but not yet strong or decisive evidence for the AP effect in the current BOSS void sample. Several factors contribute to this difference. First, we do not yet have access to the full BOSS survey, which will include more galaxies within the same survey footprint, increasing the number density and hence accessing a much larger number of small voids. Second, Lavaux & Wandelt



(2012) provided forecasts using a profile-based shape measurement technique. We found that this method results in far better ellipticity measurements but only when the number of voids in a stack exceeds a threshold of  $\sim 100$  for dense surveys and  $\sim 300$  for sparse surveys within relatively narrow radius bins — otherwise the fit fails catastrophically with high probability. The redshift width of our volume-limited samples prevents us from forming stacks of the required number of voids. Finally, the earlier study used extrapolated abundances from voids found in the dark matter particle distribution rather than the more realistic simulations of voids found using dark matter halos or HOD galaxies as tracers (e.g. Furlanetto & Piran 2006; Jennings et al. 2013; Sutter et al. 2013).

Our analysis of the AP test in void catalogs drawn from realistic mocks shows that the data quality is about to cross a threshold where the AP test based on stacked voids will yield competitive and complementary measurements to those based on BAO. All that is needed is more voids to enhance the signal-to-noise, add more independent stacks, and allow measurements at higher redshifts. The BOSS survey itself will provide more voids with upcoming data releases, and future spectroscopic surveys such as WFIRST (Spergel et al. 2013), Euclid (Laureijs et al. 2011), or the Square Kilometer Array (Jarvis 2007) will dramatically increase the number of known voids from thousands to millions, allowing this analysis to move from detection of the effects to precision constraints and measurements of fundamental cosmological parameters.

## ACKNOWLEDGMENTS

The authors acknowledge support from NSF Grant NSF AST 09-08693 ARRA. BDW acknowledges funding from an ANR Chaire d'Excellence (ANR-10-CEXC-004-01), the UPMC Chaire Internationale in Theoretical Cosmology, and NSF grants AST-0908 902 and AST-0708849. This work made in the ILP LABEX (under reference ANR-10-LABX-63) was supported by French state funds managed by the ANR within the Investissements d'Avenir programme under reference ANR-11-IDEX-0004-02. The authors thank Qingqing Mao for suggesting the ellipticity measurement method and Nico Hamaus, Guilhem Lavaux, and David Weinberg for useful comments and discussion.

## REFERENCES

1961, *The Theory of Probability*. Oxford University Press, Oxford, England  
 Abazajian K. N., et al., 2009, *Astrophys. J. Supp.*, 182, 543  
 Ahn C. P., et al., 2014, *Astrophys. J. Supp.*, 211, 17  
 Alcock C., Paczyński B., 1979, *Nature*, 281, 358  
 Aldering G., et al., 2002, *Future Research Direction and Visions for Astronomy*. Edited by Dressler, 4835, 146  
 Anderson L., et al., 2012, *ArXiv e-prints*: 1203.6594  
 Berlind A. A., Weinberg D. H., 2002, *ApJ*, 575, 587  
 Blake C., et al., 2011, *Mon. Not. R. Astron. Soc.*, 418, 1725  
 Eriksen K. A., Marble A. R., Impey C. D., Bai L., Petry C. E., 2005, *Observing Dark Energy*, 339  
 Furlanetto S. R., Piran T., 2006, *Mon. Not. R. Astron. Soc.*, 366, 467

Hamaus N., Sutter P. M., Wandelt B. D., 2014, *ArXiv e-prints*: 1403.5499  
 Hamaus N., Wandelt B. D., Sutter P. M., Lavaux G., Warren M. S., 2013, *ArXiv e-prints*: 1307.2571  
 Hui L., Stebbins A., Burles S., 1999, *ApJ*, 511, L5  
 Jarvis M. J., 2007, *At the Edge of the Universe: Latest Results from the Deepest Astronomical Surveys ASP Conference Series*, Vol. 380, proceedings of the conference held 9-13 October, 2006 at Sintra, Portugal. Edited by Jos Afonso, Henry C. Ferguson, Bahram Mobasher, and Ray Norris., p.251, 380  
 Jennings E., Baugh C. M., Pascoli S., 2012, *Mon. Not. R. Astron. Soc.*, 420, 1079  
 Jennings E., Li Y., Hu W., 2013, *ArXiv e-prints*: 1304.6087  
 Kim Y.-R., Croft R. A. C., 2007, *Mon. Not. R. Astron. Soc.*, 374, 535  
 Komatsu E., et al., 2011, *Astrophys. J. Supp.*, 192, 18  
 Laureijs R., et al., 2011, *Euclid Definition Study Report*, *arXiv*: 1110.3193  
 Lavaux G., Wandelt B. D., 2012, *ApJ*, 754, 109  
 McDonald P., Miralda-Escudé J., 1999, *ApJ*, 518, 24  
 Melchior P., Sutter P. M., Sheldon E. S., Krause E., Wandelt B. D., 2014, *Mon. Not. R. Astron. Soc.*, 440, 2922  
 Neyrinck M. C., 2008, *Mon. Not. R. Astron. Soc.*, 386, 2101  
 Nusser A., 2005, *Mon. Not. R. Astron. Soc.*, 364, 743  
 Pisani A., Lavaux G., Sutter P. M., Wandelt B. D., 2013, *ArXiv e-prints*: 1306.3052  
 Planck Collaboration 2013, *ArXiv e-prints*: 1303.5079  
 Reid B. A., et al., 2012, *Mon. Not. R. Astron. Soc.*, 426, 2719  
 Ryden B. S., 1995, *ApJ*, 452, 25  
 Ryden B. S., Melott A. L., 1996, *ApJ*, 470, 160  
 Spergel D., et al., 2013, *ArXiv e-prints*: 1305.5422  
 Sutter P. M., Elahi P., Falck B., Onions J., Hamaus N., Knebe A., Srisawat C., Schneider A., 2014, *ArXiv e-prints*: 1403.7525  
 Sutter P. M., Lavaux G., Wandelt B. D., Hamaus N., Weinberg D. H., Warren M. S., 2013, *ArXiv e-prints*: 1309.5087  
 Sutter P. M., Lavaux G., Wandelt B. D., Weinberg D. H., 2012a, *ApJ*, 761, 187  
 Sutter P. M., Lavaux G., Wandelt B. D., Weinberg D. H., 2012b, *ApJ*, 761, 44  
 Sutter P. M., Lavaux G., Wandelt B. D., Weinberg D. H., Warren M. S., 2013, *ArXiv e-prints*: 1310.7155  
 Sutter P. M., Lavaux G., Wandelt B. D., Weinberg D. H., Warren M. S., 2014, *Mon. Not. R. Astron. Soc.*, 438, 3177  
 Thompson L. A., Gregory S. A., 2011, *ArXiv e-prints*: 1109.1268  
 Weinberg D. H., Mortonson M. J., Eisenstein D. J., Hirata C., Riess A. G., Rozo E., 2013, *Physics Reports*, 530, 87